Carbon 206 (2023) 314–324

Contents lists available at ScienceDirect

Carbon

journal homepage: www.elsevier.com/locate/carbon

Dual role of graphene as support of ligand-stabilized palladium nanoparticles and carbocatalyst for (de)hydrogenation of N-heterocycles

Andrés Mollar-Cuni [a], Santiago Martín [b,c,d], Gregorio Guisado-Barrios [e,**], Jose A. Mata [a,*]

[a] Institute of Advanced Materials (INAM), Centro de Innovación en Química Avanzada (ORFEO-CINQA), Universitat Jaume I, Avda. Sos Baynat S/n, 12006, Castellón, Spain
[b] Instituto de Nanociencia y Materiales de Aragón (INMA), CSIC-Universidad de Zaragoza, 50009, Zaragoza, Spain
[c] Departamento de Química Física, Universidad de Zaragoza, 50009, Zaragoza, Spain
[d] Laboratorio de Microscopias Avanzadas (LMA), Universidad de Zaragoza, Edificio I+D+i, 50018, Zaragoza, Spain
[e] Departamento de Química Inorgánica. Instituto de Síntesis Química y Catálisis Homogénea (ISQCH), CSIC-Universidad de Zaragoza, 50009, Zaragoza, Spain

ARTICLE INFO

Keywords:
Palladium nanoparticles
Carbocatalysis
Hydrogenation
Dehydrogenation
Supported nanoparticles
N-heterocycles
Graphene
Hydrogen storage

ABSTRACT

The hybrid material composed of palladium nanoparticles (PdNPs) functionalized with N-heterocyclic carbene ligands (NHCs) immobilized onto the surface of reduced graphene oxide (**rGO**) results in an efficient catalytic material towards hydrogenation and dehydrogenation of N-heterocycles. The **rGO** plays a dual role by acting as a carbocatalyst in acceptorless dehydrogenation of N-heterocycles and as a support for the palladium nanoparticles facilitating its interaction with molecular hydrogen turning this hybrid material into an effective hydrogenation catalyst. Hot filtration experiments support the heterogeneous nature of the process underlining the strong interaction of palladium nanoparticles with the graphene enabled by π-interactions of the ligand with the support. The mild conditions used in both transformations of this system without requiring any additives facilitates its potential application in hydrogen storage technologies in the form of liquid organic hydrogen carriers (LOHCs). At the same time, the hybrid material is a robust and efficient catalytic platform that can be recovered and reused up to eight runs in both transformations without significant deactivation. The use of a single solid catalysts that is recyclable in hydrogen conversion and reconversion through (de)hydrogenation of N-heterocycles paves the way for the development of efficient hydrogen storage materials.

1. Introduction

The principle of microscopic reversibility states that catalytic reactions are essentially reversible as the potential energy surface does not depend on the direction of the reaction [1–3]. Herein, the mechanism is the same (but reversed) for both, the forward and backward version of the reaction. They have the same energy path and transition state but differ in the activation energy and substrate-catalyst binding affinity. As a result, catalysts are efficient in only one direction specially in thermally activated reactions. Although there are reported examples in the literature where a single catalyst is efficient in both processes, still they are predominantly limited to electro and enzymatic catalysis [4–8]. In parallel, both the hydrogenation and dehydrogenation of N-heterocycles are considered fundamental organic transformations since this class of molecules are relevant in the preparation of drugs and biologically active intermediates [9–13]. Hydrogenation of N-heterocycles is favored by thermodynamics being an exergonic reaction although not entropically favored by the conversion of H_2 gas [14–17]. On the contrary, dehydrogenation of N-heterocycles is endergonic but entropically favored and requires the removal of H_2 gas from the reaction media to proceed, which experimentally is translated in the use of high-temperature reactions and working with systems that allow the release of hydrogen [18–22].

The combination of such reversible reactions could potentially be used for hydrogen storage using organic molecules. These are the basis of the Liquid Organic Hydrogen Carrier (LOHC) technologies that enable hydrogen store in the liquid form [23–27]. The conversion of hydrogen gas into a liquid in LOHCs represents an attractive alternative for

Abbreviations: LOHC, liquid organic hydrogen carriers; rGO, reduced graphene oxide; PdNPs, palladium nanoparticles.

* Corresponding author.
** Corresponding author.
E-mail addresses: gguisado@unizar.es (G. Guisado-Barrios), jmata@uji.es (J.A. Mata).

https://doi.org/10.1016/j.carbon.2023.02.014
Received 1 November 2022; Received in revised form 17 January 2023; Accepted 11 February 2023
Available online 18 February 2023

hydrogen storage when compared to traditional high-pressure or liquified technologies [28–30]. N-heterocycles are suitable candidates to fulfill all the technical requirements for efficient LOHCs displaying lower enthalpy in the dehydrogenation process when compared with cyclic alkanes [31–36]. Thus, the availability of a single catalytic platform for hydrogen release and up-take using N-heterocycles as LOHCs is considered a valuable and promising alternative to address the current technological shortcomings.

Herein we describe the synthesis of a reversible catalytic system based on a hybrid material. The material is prepared using a bottom-up approach starting from a well-defined N-heterocyclic carbene palladium molecular complex which contains a pyrene tag that facilitates π-interactions with **rGO**. Decomposition of the immobilized complex onto the surface of graphene results in the formation of palladium nanoparticles (PdNPs) featuring homogeneous size, shape, and composition affording the hybrid material (**1-rGO-NPs**). The catalytic performance of **1-rGO-NPs** was evaluated in (de)hydrogenation of N-heterocycles. The PdNPs are the active sites in hydrogenation using H_2 and the **rGO** acts as a carbocatalyst in acceptorless dehydrogenation of N-heterocycles. The stabilization of the PdNPs by NHC ligands and the use of graphene as support enables the **1-rGO-NPs** to be used and recycled in sequential (de)hydrogenation reactions up to eight cycles. To the best of our knowledge, the combination of MNPs and a carbocatalyst into a single catalytic hybrid material has no precedent and the particularity of this performance is attributed to the dual role played by graphene.

2. Experimental section

2.1. Materials

Reagents used in the preparation of catalyst were synthetic grade and used without further purification process unless otherwise stated. Palladium (II) bromide (99%), K_2CO_3 (99%), 3-chloropyridine (99%), 1,3,5-trimethoxybenzene (99%). Solvents of HPLC grade were used without further purification: CH_2Cl_2, Diethylether, ethyl-acetate, n-pentane, ^{i}PrOH, EtOH. 1,2-DCB (1,2-Dichlorobenzene) used as solvent in dehydrogenation reactions was deoxygenated by freeze-pump-thaw method. Reduced Graphene Oxide (**rGO**) was purchased (Graphenea) and used as received. N-heterocycles are commercially available (Sigma-Aldrich) and used as received.

2.2. Catalyst preparation

Synthesis of 1: The palladium complex was prepared by adapting a previous reported procedure described by our group [37]. In brief, the imidazolium salt **A** (241 mg, 0.5 mmol), palladium(II) bromide (133 mg, 0.5 mmol), potassium carbonate (207 mg, 1.5 mmol) and 3-chloropyridine (3 mL) were introduced into a Schlenk and the resulting suspension was stirred for 20 h at 80 °C. The reaction mixture was filtered through a short pad of Celite using CH_2Cl_2 and the yellow solution was evaporated to dryness. The oily precipitate was dissolved in CH_2Cl_2 and was precipitated with n-hexanes affording a yellow solid that was filtered and washed with diethyl ether. (Yield 270 mg, 70%).

Synthesis of 1-rGO: A suspension of 1 g of **rGO** in 560 mL of CH_2Cl_2 was introduced in an ultrasounds bath for 30 min. Then, complex **1** (160 mg, 0.21 mmol) was added to the mixture and the suspension was stirred at room temperature for 16 h. The black solid was isolated by filtration and washed with CH_2Cl_2 (3 × 100 mL) affording the hybrid material as a black solid. The exact amount of complex supported was determined by ICP-MS analysis. The results accounted for a 5.5 wt% of complex **1** in the hybrid material **1-rGO**.

Synthesis of 1-rGO-NPs. A Schlenk flask equipped with a stirring bar was loaded with **1-rGO** (200 mg), Cs_2CO_3 (118 mg, 0.052 mmol) and toluene (24 mL). Then, a balloon of H_2 (1 bar) was connected to the Schlenk and the reaction mixture was stirred at 65 °C for 1 h. After this time, **1-rGO-NPs** were filtered, washed with toluene (3 × 30 mL), deionized water (3 × 30 mL), acetone (3 × 30 mL) and dried. **1-rGO-NPs** were characterized by HRTEM and XPS, and the exact amount of Pd on the surface of graphene was determined by ICP-MS. The results accounted for a 0.57 wt % of Pd in the hybrid material **1-rGO-NPs**.

2.3. Characterization

Nuclear magnetic resonance (NMR) spectra were recorded on Bruker spectrometers operating at 300 or 400 MHz (^{1}H NMR) and 75 or 100 MHz (^{13}C{^{1}H} NMR), respectively, and referenced to $SiMe_4$ (δ in ppm and J in Hertz). Yield and conversion were determined by a GC-2010 (Shimadzu) gas chromatograph equipped with a FID and a Teknokroma (TRB-5MS; 30 m × 0.25 mm x 0.25 mm) column. High-resolution images of transmission electron microscopy HRTEM and high-angle annular dark-field HAADF-STEM images of the samples were obtained using a Jem-2100 LaB6 (JEOL) transmission electron microscope coupled with an INCA Energy TEM 200 (Oxford) energy dispersive X-Ray spectrometer (EDX) operating at 200 kV. Samples were prepared by drying a droplet of a MeOH dispersion on a carbon-coated copper grid. X-ray photoelectron spectra (XPS) were acquired on a Kratos AXIS ultra DLD spectrometer with a monochromatic Al Kα X-ray source (1486.6 eV) using a pass energy of 20 eV. To provide a precise energy calibration, the XPS binding energies were referenced to the C1s peak at 284.6 eV. The metal content of materials was determined by inductively coupled mass spectrometry (ICP-MS) analysis. In brief, digestion of ca. 15 mg sample material was performed in a Mars 6 iWave CEM microwave oven using nitric acid (69%) with a power of 1800 W at 210 °C during 25 min. After removal of solid particles by filtration and dilution to an appropriate volume, ICP-MS analysis were recorded on an Agilent 7500 CX instrument in duplicate. TGA was performed using a TGSTDA Mettler Toledo model TGA/SDTA851e/LF/1600 coupled to a mass spectrometer quadrupole PFEIFFER VACUUM model OmniStar GSD 320 O3, 1−300 uma bearing a tungsten filament. The analysis was carried out heating ca. 15 mg of sample in alumina pan from 35 to 1100 °C at 10 °C min^{-1} using a nitrogen flow. Raman spectra were recorded at room temperature with 547 nm laser excitation focused through a WITec GmbH Raman spectrophotometer equipped with a CCD detector. FTIR spectra were recorded at room temperature employing a Jasco *FT/IR-6200* spectrophotometer with a *Jasco ATR Pro One dispositive.*

2.4. Dehydrogenation of N-heterocycles

In a general catalytic experiment, a 10 mL Schlenk flask equipped with a stirring bar was charged with 0.1 mmol of tetrahydroquinoline, catalyst (from 19 to 45 mg) and 2 mL of 1,2-dichlorobenzene under N_2. The reaction flask was equipped with a condenser and then introduced in a preheated 130 °C oil bath. The reaction was refluxed with stirring in an open system for 23 h. After cooling to room temperature, yields and conversions were determined by GC and/or ^{1}H NMR analysis using 1,3,5-trimethoxybenzene as an internal standard.

2.5. Hydrogenation of N-heterocycles

In a general catalytic experiment, a 2 mL vial equipped with a stirring bar was charged with 0.05 mmol of N-heterocycle, catalyst and 1 mL of solvent and was introduced in an autoclave. The reactor was purged 3 times with 5 bars of H_2 prior being pressurized to 15 bars and heated at 70 °C for 6 h. After this time, H_2 was released, and the reactor was left to reach room temperature. Yields and conversions were determined by GC and/or ^{1}H NMR analysis using 1,3,5-trimethoxybenzene as an internal standard.

2.6. Reusability experiments in dehydrogenation of tetrahydroquinoline

A 25 mL Schlenk equipped with a stirring bar is loaded with 0.3 mmol of tetrahydroquinoline, 84 mg of catalyst and 6 mL of 1,2-

dichlorobenzene used as solvent. The balloon is then introduced in a preheated 130 °C oil-bath for 23 h. After each run, the solid catalyst is isolated, washed with 1,2-DCB (*x*3) and ethyl-acetate (*x*3) and dried with pentane (*x*1). The solid catalyst is then used in a next run without any regeneration process. Yields and conversions were determined by GC using 1,3,5-trimethoxybenzene as an internal standard.

2.7. Reusability properties in sequential hydrogenation/dehydrogenation cycles

Hydrogenation: A 10 mL vial equipped with a stirring bar was loaded with 0.3 mmol of quinoline, **1-rGO-NPs** (1.5 mol% based on Pd, 84 mg) and 6 mL of ^{i}PrOH was introduced in an autoclave and sealed. The reactor was purged 3 times with 5 bar of H_2, then it was pressurized to 15 bars and heated at 70 °C for 3 h to achieve ca. 50% conversion. After this time, H_2 was released, and the reactor was left to reach room temperature. The solid hybrid catalyst was recovered by centrifugation, washed with ^{i}PrOH (3 × 5 mL), pentane (1 × 5 mL) and dried before it was used in the subsequent dehydrogenation run. The liquid phase was analyzed by GC chromatography for determining yield and conversion using 1,3,5-trimethoxybenzene as an internal standard.

Dehydrogenation: The recovered hybrid catalyst was further used without any regeneration process in a dehydrogenation reaction completing a (de)hydrogenation cycle. A 10 mL round bottom flask equipped with a stirring bar was charged with 0.3 mmol of tetrahydroquinoline, **1-rGO-NPs** (84 mg) and 6 mL of 1,2-dichlorobenzene. The reaction flask, equipped with a condenser, was then introduced in a preheated 130 °C oil bath. The reaction was refluxed with stirring for 6 h to afford ca. 50% conversion. After cooling to room temperature, the solid catalyst was separated by centrifugation, washed with 1,2-DCB (3 × 5 mL), ethyl-acetate (3 × 5 mL), pentane (1 × 5 mL) and dried before using it in the following hydrogenation run. Yields and conversions were determined by GC using 1,3,5-trimethoxybenzene as an internal standard. The overall sequential process hydrogenation/dehydrogenation was repeated up to four cycles (eight runs) and then the solid catalyst was analyzed by HRTEM microscopy.

2.8. Molecular hydrogen determination

A 25 mL two-necked round bottom flask equipped with a stirring bar was charged with 0.2 mmol of tetrahydroquinoline, **1-rGO-NPs** (55 mg) and 4 mL of 1,2-dichlorobenzene. The reaction flask was equipped with a condenser and then introduced in a preheated 130 °C oil bath. The reaction was refluxed with stirring in a closed system. After 5 h, a 1.5 mL sample of the evolved gas was captured with a syringe and injected in a quadrupole mass spectrometer equipment (Omnistar GSD 320 03 from PFEIFER VACUUM) confirming the presence of molecular hydrogen.

3. Results and discussion

3.1. Catalysts synthesis and characterization

Ligand-stabilized palladium nanoparticles anchored onto graphene used in (de)hydrogenation of N-heterocycles were prepared in a two-step process starting from the palladium complex **1** (Scheme 1). The design of an N-heterocyclic carbene ligand containing a polyaromatic tag allows the immobilization of complex **1** onto graphene by π-interactions [38–40]. This methodology facilitates the preparation of **1-rGO** with a controlled composition of the precursor species used for the formation of palladium nanoparticles. The presence of the polyaromatic tag is responsible for the immobilization of molecular species and metal nanoparticles onto graphene. We have previously observed that ruthenium [41–43], iridium [44], platinum [45] and gold [46,47] molecular complexes containing a pyrene tag form strong π-stacking interactions with reduced graphene oxide. The catalytic properties revealed that these interactions are maintained during reusability experiments. We have not observed deactivation promoted by leaching, which confirmed the importance of the polyaromatic group in the stability of metal species anchored onto graphene derivatives [48,49]. Exposure of the hybrid material **1-rGO** to hydrogen under mild conditions induce the formation of palladium nanoparticles anchored onto graphene (**1-rGO-NPs**). Decomposition of metal complexes for the formation of metal nanoparticles is a well stablished procedure first developed by Chaudret [50–55]. This organometallic approach allows the formation of metal nanoparticles stabilized by the presence of ligands. The ligands (NHCs) avoid aggregation and control the size and morphology of the metal nanoparticles [56–58].

The exact nature and composition of palladium nanoparticles onto graphene was determined by microscopic, spectroscopic, and analytical techniques starting from the molecular palladium complex (**1**), its immobilized version (**1-rGO**) to the final hybrid material (**1-rGO-NPs**). Supporting information contains detailed characterization information of all species. NMR spectroscopy and high-resolution mass spectrometry (HRMS) provide full characterization of **1** and the imidazolium salt **A** (Figs. S2–S6). Morphological analysis of **1-rGO** by HRTEM microscopy displays the characteristic bidimensional nature of graphene and the absence of metal aggregates in the form of palladium nanoparticles (Fig. 1a & S7). EDX analysis reveals the presence of palladium (also N, Br and Cl) homogeneously distributed on the surface of graphene confirming the presence of complex **1** onto the surface of **rGO** (Fig. S8). On the contrary, morphological analysis of **1-rGO-NPs** is completely different and shows the presence of crystalline metal aggregates (Fig. 1b). These metal aggregates correspond to spherical palladium nanoparticles of an average size of 1.98 ± 0.81 nm (Fig. 1c). Further characterization includes thermogravimetric analysis (TGA), infrared spectroscopy (FTIR) and Raman spectroscopy through comparative studies of **rGO**, **1-rGO** and **1-rGO-NPs** (Fig. 1d–f). Thermogravimetric analysis reveals a similar behavior for the three materials highlighting their stability vs. temperature under nitrogen conditions. FTIR shows comparable predominant bands for **rGO**, **1-rGO** and **1-rGO-NPs** of the carbon support. Raman spectroscopy reveals that the incorporation of the molecular complex **1** or the formation of PdNPs does not alter the relative intensity of the graphitic (1590 cm^{-1}) and defect (1350 cm^{-1}) bands. These techniques provide limited information about palladium species most probably due to the low ratio compare to the support but contribute to the characterization and changes produced in the carbon support. Further evidence of the nature, composition and properties of palladium species was obtained by X-ray photoelectron spectroscopy (XPS) analysis.

X-ray photoelectron spectroscopy (XPS) provides valuable

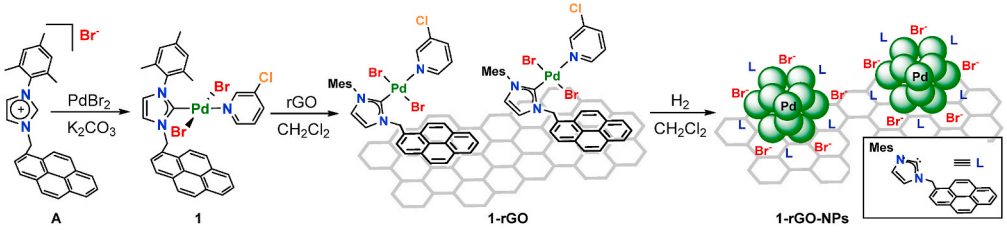

Scheme 1. Bottom-up synthesis of ligand-stabilized palladium nanoparticles supported onto graphene.

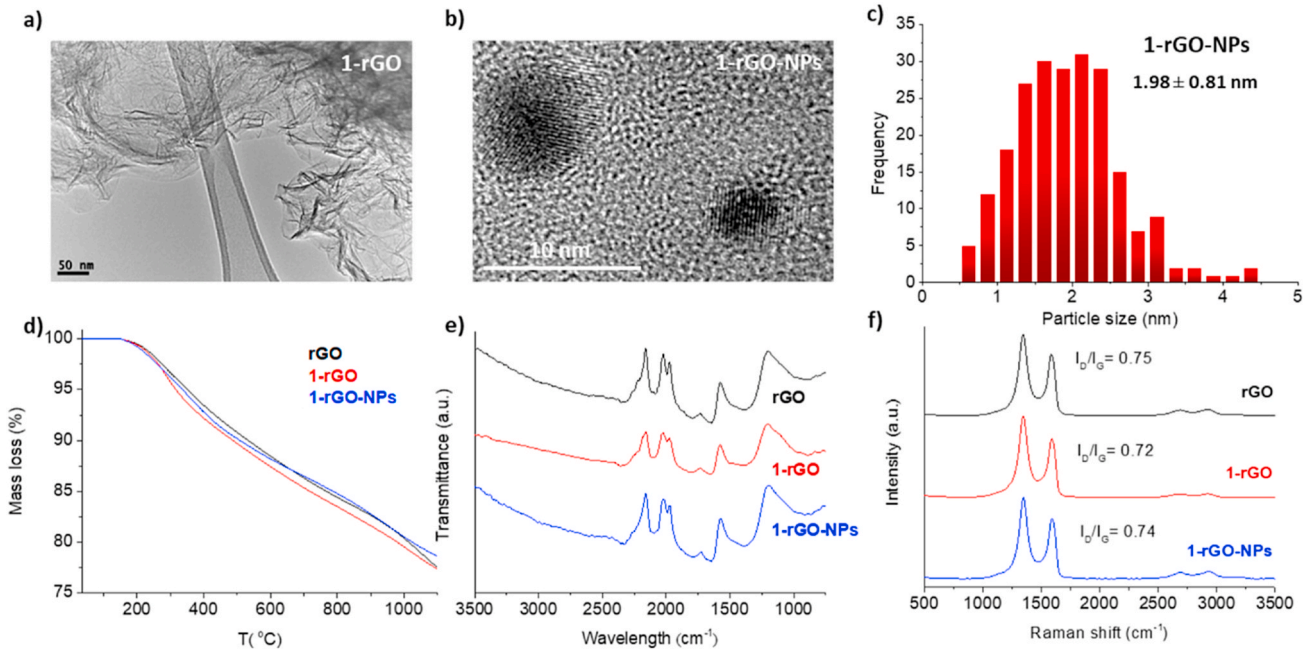

Fig. 1. Characterization of hybrid materials. a) and b) HRTEM images. c) Size histogram (n = 226) of palladium nanoparticles. d) Thermograms of graphene materials under nitrogen. e) FTIR spectra and f) Raman spectra. (A colour version of this figure can be viewed online.)

information of elemental composition, oxidation states and binding energies. This technique is particularly useful for our materials as the bottom-up approach synthetic procedure allows the XPS analysis of all the individual components. We have performed a detailed analysis of XPS data corresponding to the molecular complex **1** and all the materials involved in our catalytic system (**rGO**, **1-rGO** and **1-rGO-NPs**). XPS analysis of **1** and **1-rGO** shows the characteristic peaks corresponding Pd 3d, Br 3d, N 1s and Cl 2p at the same binding energies, confirming the immobilization of the molecular complex onto the surface of graphene (Figs. S15–S17). The high-resolution core-level peak of Pd 3d supports, as expected, a Pd^{2+} oxidation state as a doublet at 343.0 and 337.7 eV for complex **1** and at 342.9 and 337.7 eV for **1-rGO** (Fig. 2a & b). XPS analysis of **1-rGO-NPs** displays peaks (C, N and Br) at binding energies corresponding to the NHC ligand confirming its presence in the final hybrid material (Fig. S18). We have not observed the presence of Cl, indicating that the 3-chloropyridine ligand is lost during the nucleation and growing of metal nanoparticles. This is not unexpected as the 3-chloropyridine ligand is labile and likely to dissociate from the metal center. Interestingly, the high-resolution XPS analysis for the core-level peaks of Pd3d of **1-rGO-NPs** displays two doublets confirming the presence of Pd^0 and Pd^{2+} oxidation states (Fig. 2c). Our approach represents a convenient methodology for the preparation of hybrid materials with an exhaustive control on composition and correlation between the different components. We propose a model for the **1-rGO-NPs** material that consists of reduced graphene oxide decorated with small and spherical palladium nanoparticles. The Pd NPs contain Pd^0 atoms at the core and Pd^{2+} ions at the surface coordinated to NHC and Br ligands.

3.2. Dehydrogenation of N-heterocycles

The activity of **1-rGO-NPs** as catalyst for dehydrogenation of N-heterocycles was initially assessed using 1,2,3,4-tetrahydroquinoline as model substrate (Table 1). Dehydrogenation is endergonic and requires high temperatures to proceed. For this reason, we first evaluated the reaction without any catalyst (Table 1, entry 1). No conversion nor trace of quinoline was detected by gas chromatography (GC/FID) analysis indicating the need of a catalysts and highlighting the stability of 1,2,3,4-tetrahydroquinoline under the reaction conditions. Control

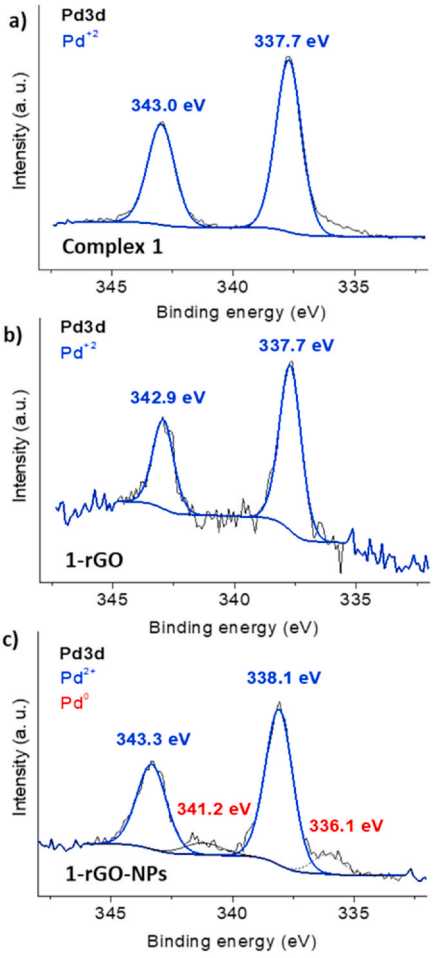

Fig. 2. Comparative XPS analysis of the core-level peak of Pd3d for the different palladium species. (A colour version of this figure can be viewed online.)

Table 1
Dehydrogenation of 1,2,3,4-tetrahydroquinoline.

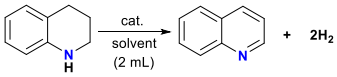

Entry	Cat.	Solvent	T (ºC)	Time (h)	Conv. (%)	Productivity $*10^{-6}$ (mol/g_{cat}h)
1	-	1,2-DCB	130	23	–	–
2	**1**	1,2-DCB	130	7	5	19
3	**rGO**	1,2-DCB	130	9	80	234
4	**1-rGO**	1,2-DCB	130	9	82	240
5	**1-rGO-NPs**	1,2-DCB	130	9	83	243
6	**1-rGO-NPs**	toluene	130	9	40	117
7	**1-rGO-NPs**	toluene	130	23	60	69
8	**1-rGO-NPs**	*p*-xylene	130	9	71	208
9	**1-rGO-NPs**	*p*-xylene	130	23	99	113
10	**1-rGO-NPs**	1,2-DCB	130	23	100	114
11	**1-rGO-NPs**	1,2-DCB	110	23	60	69
12	**1-rGO-NPs**	1,2-DCB	110	48	100	55
13	**1-rGO-NPs**	1,2-DCB	100	23	5	6
14[a]	**1-rGO-NPs**	1,2-DCB	130	20	7	9

Reaction conditions: 1,2,3,4-tetrahydroquinoline (0.10 mmol), catalyst loading (38 mg), solvent (2 mL). Conversion determined by GC using 1,3,5-trimethoxybenzene as an internal standard. a) reaction performed in a closed vessel.

experiments using only the molecular palladium **1** exclude this complex as a competent catalyst for this transformation and reveal that graphene species are required to promote dehydrogenation of tetrahydroquinolines (Table 1, entry 2). In fact, when using reduced graphene oxide (**rGO**) a yield of 80% of quinoline is obtained indicating that graphene acts as an efficient carbocatalysts as we and others have previously observed for this and related carbonaceous materials [59–63]. Comparison of the catalytic activity of **rGO** with palladium in the form of molecular species (**1-rGO**) or nanoparticles (**1-rGO-NPs**) reveal that no significant differences are observed (Table 1, entries 3–5). These results reinforce the role of **rGO** as carbocatalysts and point out that the palladium species do not have any effect in the catalytic dehydrogenation of tetrahydroquinolines. The dehydrogenation of 1,2,3,4-tetrahydroquinoline proceeds using different solvents such as toluene, *p*-xylene or 1,2-DCB (Fig. S19). However, low to moderate activity was observed when toluene was used as solvent (Table 1, entries 6–7), but it was significantly superseded with *p*-xylene (entries 8–9). Still, the best results of 70% conversion in 9 h (and 100% in 23 h) were obtained when using 1,2-DCB (Table 1, entries 5, 10). The reaction temperature strongly influences the catalytic activity. For instance, at 130 °C full conversion to quinoline was obtained in 23 h (Table 1, entry 10). In contrast, when the reaction was carried out at 110 °C the conversion lowers to 60% (Table 1, entry 11) and requires 48 h to reach full conversion (Table 1, entry 12). Furthermore, it was observed that the dehydrogenation of N-heterocycles was negligible at 100 °C or below (Table 1, entry 13). In addition, we have observed that dehydrogenation of 1,2,3,4-tetrahydroquinoline does not evolve when using a closed system that impedes the release of H_2 (Table 1, entry 14).

To further explore the catalytic properties of **1-rGO-NPs**, dehydrogenation of 1,2,3,4-tetrahydroquinoline was evaluated at different catalyst loadings at 130 °C in 1,2-DCB (Fig. 3a). Assessment of catalyst loading provides valuable information regarding the implication of the catalyst in the kinetics of the process. Using a catalyst loading of 45 mg, 1,2,3,4-tetrahydroquinoline is quantitatively dehydrogenated (95%) in 9 h. Notably, lowering the catalyst loading to 28 mg affords quantitative yields in 23 h highlighting the stability of the catalyst. We used these data to establish the catalytic reaction order using variable time normalization analysis (VTNA); a graphical method that uses reaction progress profiles [64–66]. The results suggest a first-order dependence in catalyst, providing evidence that this species are involved in the rate-determining step of the reaction and that the diffusion factors do not play an important role (Fig. S21). In order to exclude any diffusional limitations, we monitored reaction profiles at different stirring speeds (Fig. 3b) [67]. The results illustrate that reaction rates are not altered under different conditions indicating the absence of mass transfer limitations in our catalytic system.

The scope of dehydrogenation was studied using different N-heterocycles and monitoring the yield/conversion of the reaction vs. time (Fig. 4). Palladium nanoparticles anchored onto graphene (**1-rGO-NPs**) is an efficient catalyst for dehydrogenation of different N-heterocycles such as substituted tetrahydroquinolines, tetrahydroquinoxaline and indoline. The good relationship between conversion/yield implies that all substrate is converted into the corresponding product emphasizing

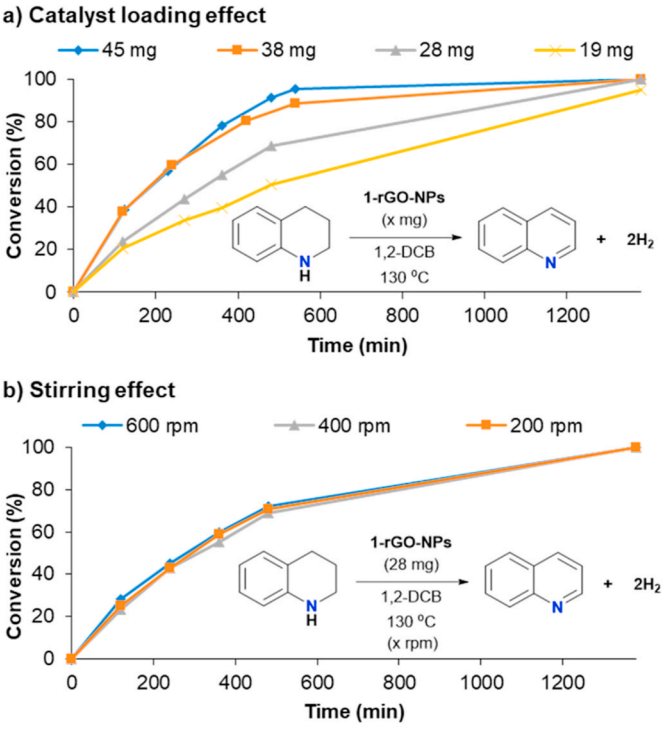

Fig. 3. Influence of catalyst loading in dehydrogenation of N-heterocycles (a) and stirring effect (b) in revolutions per minute (rpm). Conditions: 0.1 mmol of 1,2,3,4-tetrahydroquinoline, 2 mL 1,2-DCB, 130 °C and catalyst. Conversion determined by GC using 1,3,5-trimethoxybenzene as an internal standard. (A colour version of this figure can be viewed online.)

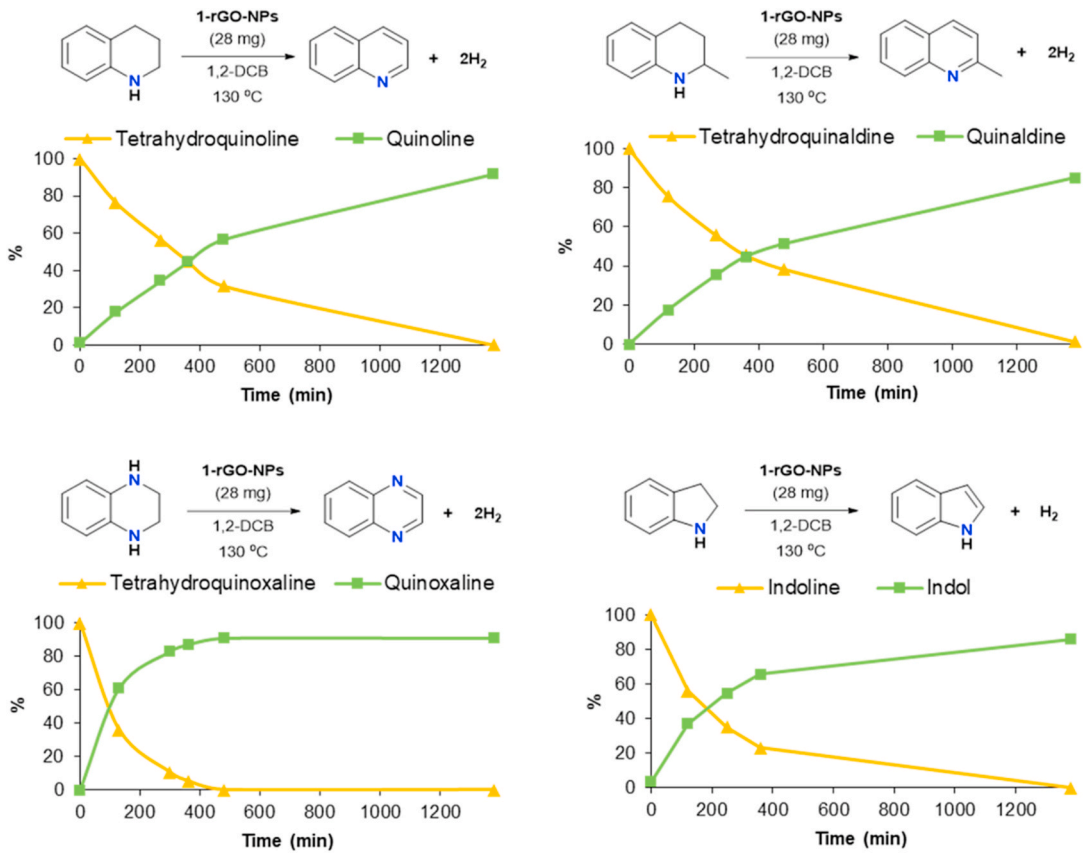

Fig. 4. Dehydrogenation of N-heterocycles catalyzed by **1-rGO-NPs**. Conditions: 0.1 mmol of substrate, 2 mL of 1,2-DCB, 130 °C and 28 mg of cat. Conversion and yield determined by GC analysis using 1,3,5-trimethoxybenzene as an internal standard. (A colour version of this figure can be viewed online.)

the selectivity of the reaction. The dehydrogenation of substituted tetrahydroquinolines reached quantitative yields (>95%) in 23 h. Indoline is also dehydrogenated in ca. 23 h but initial rates are faster and 80% yield is achieved in 6 h. However, the reaction is faster for tetrahydroquinoxaline that reached quantitative yield in 8 h. The reaction progress profiles indicate that the catalysts **1-rGO-NPs** is stable under the conditions and no deactivation is observed.

The reusability properties and stability of catalyst **1-rGO-NPs** were assessed using 1,2,3,4-tetrahydroquinoline as model substrate under standard conditions (Fig. 5 & S23). After each run, the solid catalyst was isolated by centrifugation and washed with 1,2-DCB, ethyl-acetate and n-pentane. Once the catalyst was air-dried, it was reused in a subsequent run without any regeneration process. Reaction progress profiles show a considerable decrease of activity for the second run although still quantitative conversion was obtained after 23 h. Then, activity was maintained within experimental error up to ten runs with a gradual deactivation. For instance, the conversion for run 3 is 42% after 8 h and for run 7 the conversion is 39%. It is important to note that an abrupt decay in conversion vs. time plot, implies fast catalyst deactivation by means of different processes such as decomposition, sintering or formation of inactive species. In our case, the gradual deactivation of the catalysts could be due to an experimental error in the treatment of the catalyst from run to run. The heterogenous nature of the catalyst was assessed by hot filtration experiments confirming that no active species are released from the solid into solution (Fig. S24). The reusability experiments reveal that catalyst **1-rGO-NPs** is stable and can be easily isolated and reused in multiple runs.

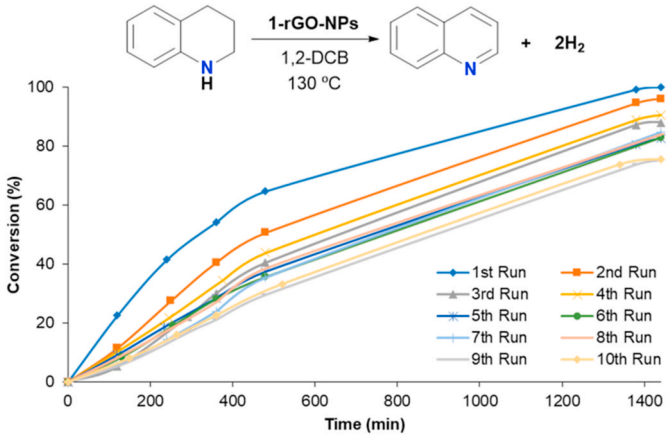

Fig. 5. Reusability properties of **1-rGO-NPs** in dehydrogenation of 1,2,3,4-tetrahydroquinoline. Conversion determined by GC analysis using 1,3,5-trimethoxybenzene as internal standard. (A colour version of this figure can be viewed online.)

3.3. *Hydrogenation of N-heterocycles*

After having assessed the catalytic properties of the hybrid material **1-rGO-NPs** in dehydrogenation of N-heterocycles, we explored the potential of this material in the hydrogenation of quinolines (*i.e.*, the reverse reaction). In a first set of reactions the activity of **1-rGO-NPs** as catalyst precursor in hydrogenation was assessed using quinoline as model substrate (Table 2). Blank experiments reveal that the presence of the catalyst is required for hydrogenation of quinoline (Table 2, entry 1). We assessed the activity of **rGO** in quinoline hydrogenation under various conditions. The results show that **rGO** used as support of PdNPs is not active in hydrogenation (Table 2, entry 2). Our studies in (de) hydrogenation of N-heterocycles establish that **rGO** is an efficient

Table 2
Hydrogenation of quinoline under various conditions.

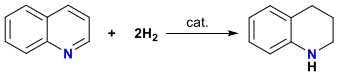

Entry	Cat.	Loading (mol%)	Solvent	Yield (%)[a]	TOF_m (h^{-1})[b]
1	-	-	EtOH	0	–
2	**rGO**	20 mg	EtOH	0	–
3	**1-rGO-NPs**	1.5	1,2-DCB	0	–
4	**1-rGO-NPs**	1.5	toluene	3	0.4
5	**1-rGO-NPs**	1.5	H_2O	10	1.2
6	**1-rGO-NPs**	1.5	EtOH	95	10.6
7	**1-rGO-NPs**	1.5	^{i}PrOH	100	11.2
8	**1-rGO-NPs**	1	^{i}PrOH	75	12.5
9	**1-rGO-NPs**	0.75	^{i}PrOH	68	15.1
10	**1-rGO-NPs**	0.5	^{i}PrOH	60	20.0

Reaction conditions: quinoline (0.05 mmol), catalyst loading in mol% based on Pd, P(H_2) 15 bar, solvent (1 mL), 70 °C for 6 h [a]Yields determined by GC using 1,3,5-trimethoxybenzene as an internal standard. [b]TOF_m at 6 h considering all the palladium in the reaction media and not only the one located at the surface of PdNPs.

carbocatalyst in dehydrogenation but not in the reverse hydrogenation reaction. The hydrogenation of N-heterocycles and particularly quinoline, requires the presence of PdNPs as active catalytic sites. For instance, we have observed that hydrogenation of quinoline using **1-rGO-NPs** as catalysts is solvent dependent. While conversions were zero or very low using 1,2-DCB, toluene or water as solvents (Table 2, entries 3–5), a high yield of tetrahydroquinoline (95%) was obtained when using EtOH (Table 2, entry 6). The use of other alcohols such as ^{i}PrOH, were also very convenient for hydrogenation of quinoline providing quantitative yields under the same reaction conditions (Table 2, entry 8). We assessed the involvement of a transfer hydrogenation process instead of a direct hydrogenation using molecular hydrogen. We ruled out the participation of transfer hydrogenation as the reaction conversion was negligible when using a H_2 pressure of 1 bar. The best results were obtained when using an alcohol as solvent (EtOH or ^{i}PrOH) at 70 °C and a hydrogen pressure of 15 bar. Then, we assessed the scope and limitations of **1-rGO-NPs** in hydrogenation of various N-heterocycles under the optimized conditions (Table 3). The catalytic hydrogenation provides quantitative yields with high selectivity in most cases in just 6 h reaction. We have just observed low yields in the case of indoline (Table 3, entry 4) and 8-phenylquinoline (Table 3, entry 7). At this point we do not have a proper explanation for such observations but our results agree with previous reports in the hydrogenation of these substrates [8]. Nevertheless, hydrogenation of quinolines is a fast, general and selective transformation using **1-rGO-NPs** as catalyst.

Table 3
Reaction scope in hydrogenation of quinolines using **1-rGO-NPs**.

Entry	Substrate	Product	Yield (%)[a]	TOF_m (h^{-1})[b]
1	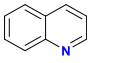		100	39.6
2	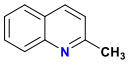	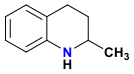	98	39.42
3			62	34.8
4			26	21.4
5	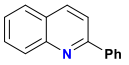	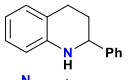	94	36.4
6			99	42.8
7			30	25.2

Reaction conditions: quinoline (0.05 mmol), catalyst (1.5 mol% based on Pd), P(H_2) 15 bar, ^{i}PrOH (1 mL), for 6 h. [a]Yields determined by GC using 1,3,5-trimethoxybenzene as an internal standard. [b]TOF_m at 1 h considering all the palladium in the reaction media and not only the one located at the surface of PdNPs.

3.4. Sequential hydrogenation/dehydrogenation of N-heterocycles

Once the properties of 1-rGO-NPs as a carbocatalyst in dehydrogenation and as a metal-based catalyst in hydrogenation of N-heterocycles have been established, we evaluated its ability in both, (de)hydrogenation cycles to assess the reusability of the catalytic system (Fig. 6). The hybrid material 1-rGO-NPs was reused in sequential hydrogenation and dehydrogenation reactions. After each run, the catalyst was isolated and used again without any regeneration process. The hydrogenation reaction was stopped at ca. 50% conversion (3 h) to detect any potential deactivation process in the following runs. It is important to note that increasing the time, the reaction achieves completeness as previously described (Tables 2 and 3). The results show that when stopping the reaction after 3 h the activity of 1-rGO-NPs remains constant at 45 ± 4% conversion (Fig. 6c, blue bars). After each hydrogenation, the catalyst was used in a dehydrogenation reaction (Fig. 6c, red bars). The dehydrogenation reaction was stopped also at ca. 50% conversion (6 h). The results show that the activity of 1-rGO-NPs remains constant at 60 ± 5% conversion. Following this procedure, after completing 4 cycles (8 runs) the hybrid material was analyzed by HRTEM microscopy and XPS spectroscopy. HRTEM and STEM images show that the morphology of 1-rGO-NPs is preserved including the bidimensional character of rGO and the presence of spherical palladium nanoparticles (Figs. S25–S28). Size analysis of palladium nanoparticles reveals a broader particle distribution compared to the fresh catalyst and a slight sintering or agglomeration process that after eight catalytic runs, increases the average size up to 7.62 ± 3.21 nm (Fig. 6e). XPS analysis of 1-rGO-NPs after reusability experiments confirms the presence of the same elements and at the same binding energy than the fresh catalyst (Fig. S29). The main difference observed by XPS analysis corresponds to the Pd^{2+}/Pd^{0} ratio (Fig. 6d). In the fresh catalyst the predominant species is Pd^{2+}, but after eight runs the dominant species is Pd^{0}. This result is rationalized by the increment of average size of PdNPs resulting in a decrease of the specific surface area and consequently decreasing the amount of Pd^{2+}. We have previously observed a similar behavior with other PdNPs anchored onto graphene [37]. The results confirm that the conditions used in both transformations do not alter significantly the catalytic activity of 1-rGO-NPs as carbocatalyst and as metal catalyst, however the size and Pd^{2+}/Pd^{0} ratio of metal nanoparticles fluctuate to some extent. Metal nanoparticles and especially PdNPs should not be considered as static species under catalytic transformations and there are precedents that highlight their dynamic character in the way of action as a "cocktail of catalysts" [68–70]. Characterization of 1-rGO-NPs before and after reusability experiments focused on the carbon support illustrate that the properties of rGO are not significantly altered during reusability experiments (Fig. 7). Thermogravimetric analysis reveals a similar mass loss for the fresh and spent material up to 1000 °C under nitrogen conditions. Raman spectroscopy displays similar relative intensities of graphitic and defect bands upon excitation at 547 nm. XPS analysis shows that deconvolution of high-resolution C1s core-level peak is maintained after reusability experiments. These results underpin the suitability of the carbon material as support of palladium nanoparticles in (de)hydrogenation processes due to its stability and capacity to avoid sintering of metal species.

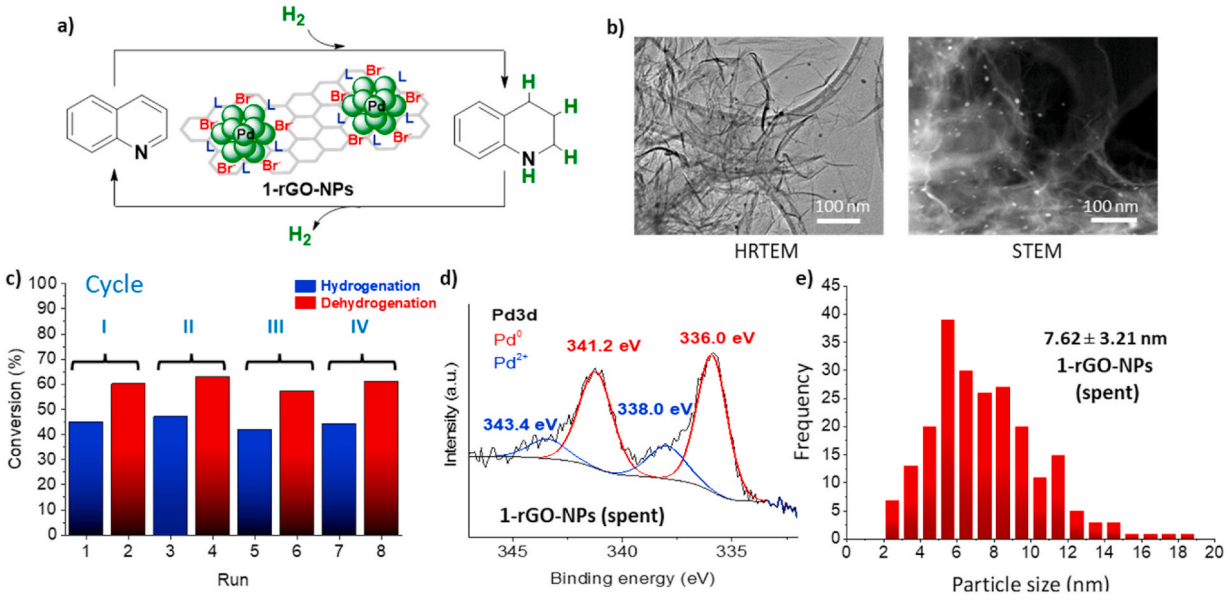

Fig. 6. a) Reaction scheme in (de)hydrogenation cycles. b) HRTEM and STEM images of **1-rGO-NPs** after reusability experiments. c) Reusability properties of **1-rGO-NPs** in sequential hydrogenation of quinoline and dehydrogenation of 1,2,3,4-tetrahydroquinoline. Catalyst 84 mg. Hydrogenation: quinoline (0.3 mmol), $P(H_2)$ 15 bar, ^{i}PrOH (6 mL), for 3 h. Dehydrogenation: 1,2,3,4-tetrahydroquinoline (0.3 mmol), 6 mL 1,2-DCB, 130 °C for 6 h. Conversions determined by GC analysis using 1,3,5-trimethoxybenzene as an internal standard. d) XPS analysis of the core-level peak of Pd3d after reusability experiments. e) Size histogram (n = 224) of palladium nanoparticles after reusability experiments. (A colour version of this figure can be viewed online.)

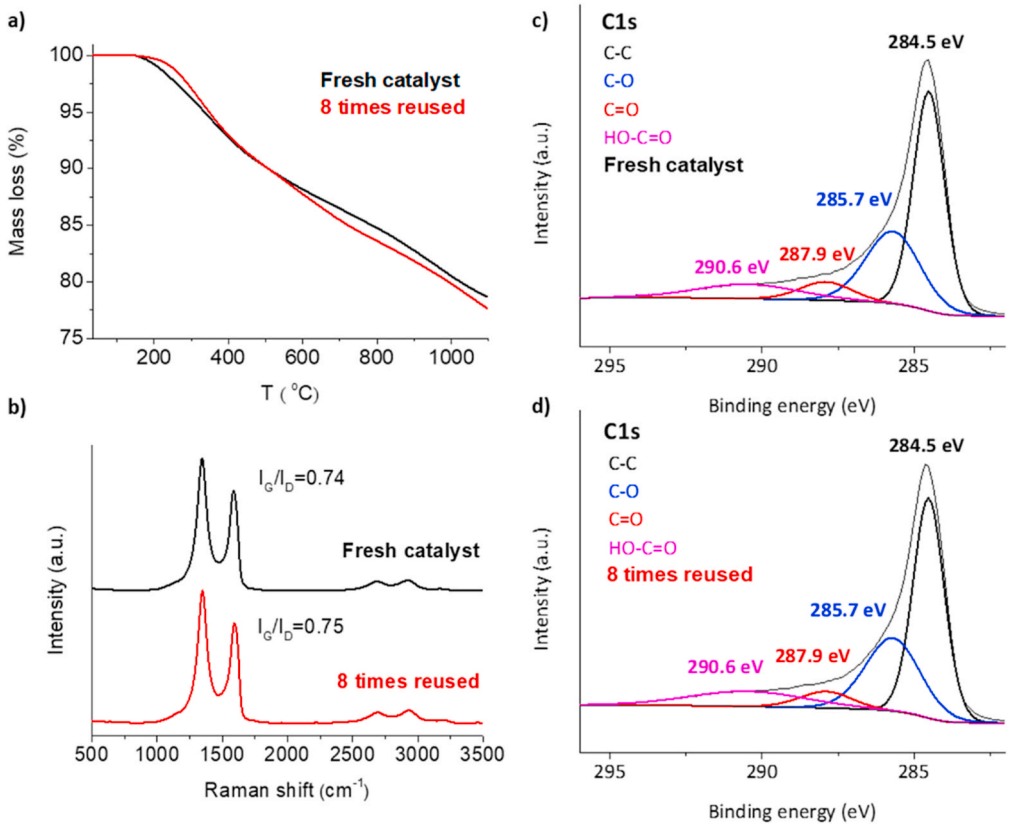

Fig. 7. Characterization of 1-rGO-NPs before and after reusability experiments focus on the carbon support. a) Thermogravimetric analysis (TGA). b) Raman spectroscopy analysis. c) & d) high-resolution XPS analysis of C1s core-level peak. (A colour version of this figure can be viewed online.)

4. Conclusions

We have developed a hybrid material composed of palladium nanoparticles stabilized with a N-heterocyclic carbene ligands containing a pyrene tag which are supported on the surface of reduced graphene oxide. The hybrid material is an efficient catalytic platform for acceptorless dehydrogenation and hydrogenation of N-heterocycles without additives. The catalytic system is robust and can be reused and recycled without reactivation processes for eight runs without significant loss of activity. The use of a single solid catalyst for the reversible (de)hydrogenation reaction of liquid organic compounds auspicious great potential for hydrogen storage in N-heterocycles. Further work for improving the catalyst performance at low temperatures in dehydrogenation and seeking other liquid organic hydrogen carriers for developing practical applications of hydrogen storage in the form of LOHCs are in progress.

Funding sources

MICIU/AEI/FEDER (PID2021-126071OB-C22 and PID2021-122900NB-I00). Universitat Jaume I (UJI-B2018-23). Generalitat Valenciana (ACIF/2019/100). RYC2019-026693-I/AEI/10.13,039/501100011033.

CRediT authorship contribution statement

Andrés Mollar-Cuni: experimental work and characterization, The manuscript was written through contributions of all authors, All authors have given approval to the final version of the manuscript, Writing – original draft, Writing – review & editing. **Santiago Martín:** experimental work and characterization, The manuscript was written through contributions of all authors, All authors have given approval to the final version of the manuscript, Writing – original draft, Writing – review & editing. **Gregorio Guisado-Barrios:** supervised the work and directed the research, The manuscript was written through contributions of all authors, All authors have given approval to the final version of the manuscript, Writing – original draft, Writing – review & editing, Supervision. **Jose A. Mata:** supervised the work and directed the research, The manuscript was written through contributions of all authors, All authors have given approval to the final version of the manuscript, Writing – original draft, Writing – review & editing, Supervision.

Declaration of competing interest

The authors declare that they have no known competing financial interests or personal relationships that could have appeared to influence the work reported in this paper.

Acknowledgements

Thanks to PID2021-126071OB-C22 and PID2021-122900NB-I00 funded by MICIN/AEI/10.13039/501100011033/FEDER “Una manera de hacer Europa”. Generalitat Valenciana (PROMETEU/2020/028) and Universitat Jaume I (UJI-B2018-23). A. M-C. thanks Generalitat Valenciana for grant (ACIF/2019/100). The authors thank ‘Servei Central d’Instrumentació Científica (SCIC) de la Universitat Jaume I’. G. G.-B gratefully acknowledges (RYC2019-026693-I/AEI/10.13039/501100011033) “El Fondo Social Europeo invierte en tu futuro’ and, with S. M., to the Gobierno de Aragón/FEDER, UE (GA/FEDER, Reactividad y catálisis en química inorgánica, Group E50_20D and E31_20 R, respectively). The authors would like to acknowledge the use of ‘Servicio General de Apoyo a la Investigación-SAI, Universidad de Zaragoza’.

Appendix A. Supplementary data

Supplementary data to this article can be found online at https://doi.org/10.1016/j.carbon.2023.02.014.

Experimental details, full characterization of materials, HRTEM images, XPS analysis, additional catalytic experiments, and spectroscopic characterization of organic products.

References

[1] R.C. Tolman, The principles of statistical mechanics, Philos. Sci. 6 (1939), https://doi.org/10.1086/286579, 381–381.
[2] E. Roduner, Understanding catalysis, Chem. Soc. Rev. 43 (2014) 8226–8239, https://doi.org/10.1039/C4CS00210E.
[3] R.D. Astumian, Trajectory and cycle-based thermodynamics and kinetics of molecular machines: the importance of microscopic reversibility, Acc. Chem. Res. 51 (2018) 2653–2661, https://doi.org/10.1021/acs.accounts.8b00253.
[4] P.J. Bonitatibus, S. Chakraborty, M.D. Doherty, O. Siclovan, W.D. Jones, G. L. Soloveichik, Reversible catalytic dehydrogenation of alcohols for energy storage, Proc. Natl. Acad. Sci. USA 112 (2015) 1687–1692, https://doi.org/10.1073/pnas.1420199112.
[5] R. Yamaguchi, C. Ikeda, Y. Takahashi, K. Fujita, Homogeneous catalytic system for reversible Dehydrogenation−Hydrogenation reactions of nitrogen heterocycles with reversible interconversion of catalytic species, J. Am. Chem. Soc. 131 (2009) 8410–8412, https://doi.org/10.1021/ja9022623.
[6] S. Chakraborty, W.W. Brennessel, W.D. Jones, A molecular iron catalyst for the acceptorless dehydrogenation and hydrogenation of N-heterocycles, J. Am. Chem. Soc. 136 (2014) 8564–8567, https://doi.org/10.1021/ja504523b.
[7] K. Kaneda, Y. Mikami, T. Mitsudome, T. Mizugaki, K. Jitsukawa, Reversible dehydrogenation-hydrogenation of tetrahydroquinoline-quinoline using a supported cooper nanoparticle catalyst, Heterocycles 82 (2010) 1371–1377, https://doi.org/10.3987/COM-10-S(E)90.
[8] X. Cui, Z. Huang, A.P. van Muyden, Z. Fei, T. Wang, P.J. Dyson, Acceptorless dehydrogenation and hydrogenation of N- and O-containing compounds on Pd 3 Au 1 (111) facets, Sci. Adv. 6 (2020) 1–11, https://doi.org/10.1126/sciadv.abb3831.
[9] J. Zhang, D. Li, G. Lu, T. Deng, C. Cai, Reversible dehydrogenation and hydrogenation of N-heterocycles catalyzed by bimetallic nanoparticles encapsulated in MIL-100(Fe), ChemCatChem 10 (2018) 4966–4972, https://doi.org/10.1002/cctc.201801311.
[10] D. Ventura-Espinosa, J.A. Mata, Multiple-metal (De-)Hydrogenation-Catalysed processes, Eur. J. Inorg. Chem. 17 (2016) 2667–2675, https://doi.org/10.1002/ejic.201600090.
[11] H. Li, J. Jiang, G. Lu, F. Huang, Z.-X. Wang, On the “reverse Gear”Mechanism of the reversible dehydrogenation/hydrogenation of a nitrogen heterocycle catalyzed by a C p *Ir complex: a computational study, Organometallics 30 (2011) 3131–3141, https://doi.org/10.1021/om200222j.
[12] W. Zhou, Q. Tao, F. Sun, X. Cao, J. Qian, J. Xu, M. He, Q. Chen, J. Xiao, Additive-free aerobic oxidative dehydrogenation of N-heterocycles under catalysis by NiMn layered hydroxide compounds, J. Catal. 361 (2018) 1–11, https://doi.org/10.1016/j.jcat.2018.01.030.
[13] X. Xu, Y. Ai, R. Wang, L. Liu, J. Yang, F. Li, Ruthenium-catalyzed acceptorless dehydrogenative coupling of o-aminobenzyl alcohols with ketones to quinolines in the presence of carbonate salt, J. Catal. 395 (2021) 340–349, https://doi.org/10.1016/j.jcat.2020.12.016.
[14] X.B. Zhang, Z. Xi, A theoretical study of the mechanism for the homogeneous catalytic reversible dehydrogenation - hydrogenation of nitrogen heterocycles, Phys. Chem. Chem. Phys. 13 (2011), https://doi.org/10.1039/c0cp02419h.
[15] G.E. Dobereiner, A. Nova, N.D. Schley, N. Hazari, S.J. Miller, O. Eisenstein, R. H. Crabtree, Iridium-catalyzed hydrogenation of N-heterocyclic compounds under mild conditions by an outer-sphere pathway, J. Am. Chem. Soc. 133 (2011) 7547–7562, https://doi.org/10.1021/ja2014983.
[16] J. Zheng, H. Zhou, C.-G. Wang, E. Ye, J.W. Xu, X.J. Loh, Z. Li, Current research progress and perspectives on liquid hydrogen rich molecules in sustainable hydrogen storage, Energy Storage Mater. 35 (2021) 695–722, https://doi.org/10.1016/j.ensm.2020.12.007.
[17] D. He, T. Wang, T. Li, X. Wang, H. Wang, X. Dai, F. Shi, Efficient hydrogenation catalyst designing via preferential adsorption sites construction towards active copper, J. Catal. 400 (2021) 397–406, https://doi.org/10.1016/j.jcat.2021.06.025.
[18] J. Wu, D. Talwar, S. Johnston, M. Yan, J. Xiao, Acceptorless dehydrogenation of nitrogen heterocycles with a versatile iridium catalyst, Angew. Chem. Int. Ed. 52 (2013) 6983–6987, https://doi.org/10.1002/anie.201300292.
[19] E. Clot, O. Eisenstein, R.H. Crabtree, Computational structure–activity relationships in H 2 storage: how placement of N atoms affects release temperatures in organic liquid storage materials, Chem. Commun. 22 (2007) 2231–2233, https://doi.org/10.1039/B705037B.
[20] Y. Zhang, J. Wang, F. Zhou, J. Liu, An effective strategy for hydrogen supply: catalytic acceptorless dehydrogenation of N-heterocycles, Catal. Sci. Technol. 11 (2021) 3990–4007, https://doi.org/10.1039/D1CY00138H.
[21] M. Kannan, P. Barteja, P. Devi, S. Muthaiah, Acceptorless dehydrogenation of amines and alcohols using simple ruthenium chloride, J. Catal. 386 (2020) 1–11, https://doi.org/10.1016/j.jcat.2020.03.025.
[22] C. Chen, Z.-Q. Wang, Y.-Y. Gong, J.-C. Wang, Y. Yuan, H. Cheng, W. Sang, S. Chaemchuen, F. Verpoort, Cobalt embedded in nitrogen-doped porous carbon as a robust heterogeneous catalyst for the atom-economic alcohol dehydrogenation to carboxylic acids, Carbon 174 (2021) 284–294, https://doi.org/10.1016/j.carbon.2020.12.040.

[23] D. Teichmann, W. Arlt, P. Wasserscheid, R. Freymann, A future energy supply based on Liquid Organic Hydrogen Carriers (LOHC), Energy Environ. Sci. 4 (2011) 2767–2773, https://doi.org/10.1039/c1ee01454d.
[24] D. Teichmann, K. Stark, K. Müller, G. Zöttl, P. Wasserscheid, W. Arlt, Energy storage in residential and commercial buildings via liquid organic hydrogen carriers (LOHC), Energy Environ. Sci. 5 (2012) 9044–9054, https://doi.org/10.1039/c2ee22070a.
[25] P. Preuster, C. Papp, P. Wasserscheid, Liquid organic hydrogen carriers (LOHCs): toward a hydrogen-free hydrogen economy, Acc. Chem. Res. 50 (2017) 74–85, https://doi.org/10.1021/acs.accounts.6b00474.
[26] M. Markiewicz, Y.Q. Zhang, A. Bösmann, N. Brückner, J. Thöming, P. Wasserscheid, S. Stolte, Environmental and health impact assessment of Liquid Organic Hydrogen Carrier (LOHC) systems – challenges and preliminary results, Energy Environ. Sci. 8 (2015) 1035–1045, https://doi.org/10.1039/C4EE03528C.
[27] P.C. Rao, M. Yoon, Potential liquid-organic hydrogen carrier (LOHC) systems: a review on recent progress, Energies 13 (2020) 6040–6063, https://doi.org/10.3390/en13226040.
[28] P.M. Modisha, C.N.M. Ouma, R. Garidzirai, P. Wasserscheid, D. Bessarabov, The prospect of hydrogen storage using liquid organic hydrogen carriers, Energy Fuel. 33 (2019) 2778–2796, https://doi.org/10.1021/acs.energyfuels.9b00296.
[29] G. Sievi, D. Geburtig, T. Skeledzic, A. Bösmann, P. Preuster, O. Brummel, F. Waidhas, M.A. Montero, P. Khanipour, I. Katsounaros, J. Libuda, K.J. J. Mayrhofer, P. Wasserscheid, Towards an efficient liquid organic hydrogen carrier fuel cell concept, Energy Environ. Sci. 12 (2019) 2305–2314, https://doi.org/10.1039/c9ee01324e.
[30] J.-Y. Cho, H. Kim, J.-E. Oh, B.Y. Park, Recent advances in homogeneous/heterogeneous catalytic hydrogenation and dehydrogenation for potential liquid organic hydrogen carrier (LOHC) systems, Catalysts 11 (2021) 1497–1526, https://doi.org/10.3390/catal11121497.
[31] R.H. Crabtree, Nitrogen-containing liquid organic hydrogen carriers: progress and prospects, ACS Sustain. Chem. Eng. 5 (2017) 4491–4498, https://doi.org/10.1021/acssuschemeng.7b00983.
[32] S. Wang, H. Huang, C. Bruneau, C. Fischmeister, Iridium-catalyzed hydrogenation and dehydrogenation of N-heterocycles in water under mild conditions, ChemSusChem 12 (2019) 2350–2354, https://doi.org/10.1002/cssc.201900626.
[33] Á. Vivancos, M. Beller, M. Albrecht, NHC-based iridium catalysts for hydrogenation and dehydrogenation of N-heteroarenes in water under mild conditions, ACS Catal. 8 (2018) 17–21, https://doi.org/10.1021/acscatal.7b03547.
[34] G. Jaiswal, M. Subaramanian, M.K. Sahoo, E. Balaraman, A reusable cobalt catalyst for reversible acceptorless dehydrogenation and hydrogenation of N-heterocycles, ChemCatChem 11 (2019) 2449–2457, https://doi.org/10.1002/cctc.201900367.
[35] T. Zhu, M. Yang, X. Chen, Y. Dong, Z. Zhang, H. Cheng, A highly active bifunctional Ru–Pd catalyst for hydrogenation and dehydrogenation of liquid organic hydrogen carriers, J. Catal. 378 (2019) 382–391, https://doi.org/10.1016/j.jcat.2019.08.032.
[36] B. Wang, T. Yan, T. Chang, J. Wei, Q. Zhou, S. Yang, T. Fang, Palladium supported on reduced graphene oxide as a high-performance catalyst for the dehydrogenation of dodecahydro-N-ethylcarbazole, Carbon 122 (2017) 9–18, https://doi.org/10.1016/j.carbon.2017.06.021.
[37] A. Mollar-Cuni, D. Ventura-Espinosa, S. Martín, Á. Mayoral, P. Borja, J.A. Mata, Stabilization of nanoparticles produced by hydrogenation of palladium-N-heterocyclic carbene complexes on the surface of graphene and implications in catalysis, ACS Omega 3 (2018) 15217–15228, https://doi.org/10.1021/acsomega.8b02193.
[38] S. Sabater, J.A. Mata, E. Peris, Catalyst enhancement and recyclability by immobilization of metal complexes onto graphene surface by noncovalent interactions, ACS Catal. 4 (2014) 2038–2047, https://doi.org/10.1021/cs5003959.
[39] S. Sabater, J.A. Mata, E. Peris, Immobilization of pyrene-tagged palladium and ruthenium complexes onto reduced graphene oxide: an efficient and highly recyclable catalyst for hydrodefluorination, Organometallics 34 (2015) 1186–1190, https://doi.org/10.1021/om501040x.
[40] M.R. Axet, O. Dechy-Cabaret, J. Durand, M. Gouygou, P. Serp, Coordination chemistry on carbon surfaces, Coord. Chem. Rev. 308 (2016) 236–345, https://doi.org/10.1016/j.ccr.2015.06.005.
[41] D. Ventura-Espinosa, A. Carretero-Cerdán, M. Baya, H. García, J.A. Mata, Catalytic dehydrogenative coupling of hydrosilanes with alcohols for the production of hydrogen on-demand: application of a silane/alcohol pair as a liquid organic hydrogen carrier, Chem. Eur J. 23 (2017) 10815–10821, https://doi.org/10.1002/chem.201700243.
[42] D. Ventura-Espinosa, A. Marzá-Beltrán, J.A. Mata, Catalytic hydrogen production by ruthenium complexes from the conversion of primary amines to nitriles: potential application as a liquid organic hydrogen carrier, Chem. Eur J. 22 (2016) 17758–17766, https://doi.org/10.1002/chem.201603423.
[43] D. Ventura-Espinosa, C. Vicent, M. Baya, J.A. Mata, Ruthenium molecular complexes immobilized on graphene as active catalysts for the synthesis of carboxylic acids from alcohol dehydrogenation, Catal. Sci. Technol. 6 (2016) 8024–8035, https://doi.org/10.1039/C6CY01455K.
[44] D. Ventura-Espinosa, S. Sabater, A. Carretero-Cerdán, M. Baya, J.A. Mata, High production of hydrogen on demand from silanes catalyzed by iridium complexes as a versatile hydrogen storage system, ACS Catal. 8 (2018) 2558–2566, https://doi.org/10.1021/acscatal.7b04479.
[45] A. Mollar-Cuni, P. Borja, S. Martin, G. Guisado-Barrios, J.A. Mata, A platinum molecular complex immobilised on the surface of graphene as active catalyst in alkyne hydrosilylation, Eur. J. Inorg. Chem. 2020 (2020) 4254–4262, https://doi.org/10.1002/ejic.202000356.
[46] D. Ventura-Espinosa, S. Sabater, J.A. Mata, Enhancement of gold catalytic activity and stability by immobilization on the surface of graphene, J. Catal. 352 (2017) 498–504, https://doi.org/10.1016/j.jcat.2017.06.021.
[47] D. Ventura-Espinosa, S. Martín, J.A. Mata, The non-innocent role of graphene in the formation/immobilization of ultra-small gold nanoparticles functionalized with N-heterocyclic carbene ligands, J. Catal. 375 (2019) 419–426, https://doi.org/10.1016/j.jcat.2019.06.009.
[48] S. Sabater, J.A. Mata, Catalytic applications of metal complexes immobilized by non-covalent interactions onto chemically derived graphenes and related materials, in: Non-Covalent Interact. Synth. Des. New Compd., John Wiley & Sons, Inc, Hoboken, NJ, 2016, pp. 313–326, https://doi.org/10.1002/9781119113874.ch17.
[49] S. Ruiz-Botella, E. Peris, Unveiling the importance of π-stacking in borrowing-hydrogen processes catalysed by iridium complexes with pyrene tags, Chem. Eur J. 21 (2015) 15263–15271, https://doi.org/10.1002/chem.201502948.
[50] P. Lara, O. Rivada-Wheelaghan, S. Conejero, R. Poteau, K. Philippot, B. Chaudret, Ruthenium nanoparticles stabilized by N-heterocyclic carbenes: ligand location and influence on reactivity, Angew. Chem. Int. Ed. 50 (2011) 12080–12084, https://doi.org/10.1002/anie.201106348.
[51] F. Dassenoy, K. Philippot, T. Ould Ely, C. Amiens, P. Lecante, E. Snoeck, A. Mosset, M.-J. Casanove, B. Chaudret, Platinum nanoparticles stabilized by CO and octanethiol ligands or polymers: FT-IR, NMR, HREM and WAXS studies, New J. Chem. 22 (1998) 703–712, https://doi.org/10.1039/a709245h.
[52] C. Pan, F. Dassenoy, M.-J. Casanove, K. Philippot, C. Amiens, P. Lecante, A. Mosset, B. Chaudret, A new synthetic method toward bimetallic ruthenium platinum nanoparticles; composition induced structural changes, J. Phys. Chem. B 103 (1999) 10098–10101, https://doi.org/10.1021/jp992072m.
[53] T.O. Ely, C. Pan, C. Amiens, B. Chaudret, F. Dassenoy, P. Lecante, M.-J. Casanove, A. Mosset, M. Respaud, J.-M. Broto, Nanoscale bimetallic Co x Pt 1 - x particles dispersed in poly(vinylpyrrolidone): synthesis from organometallic precursors and characterization, J. Phys. Chem. B 104 (2000) 695–702, https://doi.org/10.1021/jp9924427.
[54] O. Vidoni, K. Philippot, C. Amiens, B. Chaudret, O. Balmes, J.-O. Malm, J.-O. Bovin, F. Senocq, M.-J. Casanove, Novel, spongelike ruthenium particles of controllable size stabilized only by organic solvents, Angew. Chem. Int. Ed. 38 (1999) 3736–3738, https://doi.org/10.1002/(SICI)1521-3773(19991216)38:24<3736::AID-ANIE3736>3.0.CO;2-E.
[55] D. Gonzalez-Galvez, P. Lara, O. Rivada-Wheelaghan, S. Conejero, B. Chaudret, K. Philippot, P.W.N.M. van Leeuwen, NHC-stabilized ruthenium nanoparticles as new catalysts for the hydrogenation of aromatics, Catal. Sci. Technol. 3 (2013) 99–105, https://doi.org/10.1039/C2CY20561K.
[56] J.M. Asensio, S. Tricard, Y. Coppel, R. Andrés, B. Chaudret, E. de Jesús, Synthesis of water-soluble palladium nanoparticles stabilized by sulfonated N-heterocyclic carbenes, Chem. Eur J. 23 (2017) 13435–13444, https://doi.org/10.1002/chem.201702204.
[57] E.A. Baquero, S. Tricard, J.C. Flores, E. de Jesús, B. Chaudret, Highly stable water-soluble platinum nanoparticles stabilized by hydrophilic N-heterocyclic carbenes, Angew. Chem. Int. Ed. 53 (2014) 13220–13224, https://doi.org/10.1002/anie.201407758.
[58] J.M. Asensio, S. Tricard, Y. Coppel, R. Andrés, B. Chaudret, E. de Jesús, Knight shift in 13 C NMR resonances confirms the coordination of N-heterocyclic carbene ligands to water-soluble palladium nanoparticles, Angew. Chem. Int. Ed. 56 (2017) 865–869, https://doi.org/10.1002/anie.201610251.
[59] C. Su, K.P. Loh, Carbocatalysts: graphene oxide and its derivatives, Acc. Chem. Res. 46 (2013) 2275–2285, https://doi.org/10.1021/ar300118v.
[60] A. Mollar-Cuni, D. Ventura-Espinosa, S. Martín, H. García, J.A. Mata, Reduced graphene oxides as carbocatalysts in acceptorless dehydrogenation of N -heterocycles, ACS Catal. 11 (2021) 14688–14693, https://doi.org/10.1021/acscatal.1c04649.
[61] S. Navalon, A. Dhakshinamoorthy, M. Alvaro, H. Garcia, Carbocatalysis by graphene-based materials, Chem. Rev. 114 (2014) 6179–6212, https://doi.org/10.1021/cr4007347.
[62] B.F. Machado, P. Serp, Graphene-based materials for catalysis, Catal. Sci. Technol. 2 (2012) 54–75, https://doi.org/10.1039/C1CY00361E.
[63] X. Duan, M. Xiao, S. Liang, Z. Zhang, Y. Zeng, J. Xi, S. Wang, Ultrafine palladium nanoparticles supported on nitrogen-doped carbon microtubes as a high-performance organocatalyst, Carbon 119 (2017) 326–331, https://doi.org/10.1016/j.carbon.2017.04.039.
[64] J. Burés, A simple graphical method to determine the order in catalyst, Angew. Chem. Int. Ed. 55 (2016) 2028–2031, https://doi.org/10.1002/anie.201508983.
[65] C.D.T. Nielsen, J. Burés, Visual kinetic analysis, Chem. Sci. 10 (2019) 348–353, https://doi.org/10.1039/C8SC04698K.
[66] A. Martínez-Carrión, M.G. Howlett, C. Alamillo-Ferrer, A.D. Clayton, R.A. Bourne, A. Codina, A. Vidal-Ferran, R.W. Adams, J. Burés, Kinetic treatments for catalyst activation and deactivation processes based on variable time normalization

analysis, Angew. Chem. Int. Ed. 58 (2019) 10189–10193, https://doi.org/10.1002/anie.201903878.
[67] S. Domínguez-Domínguez, Á. Berenguer-Murcia, B.K. Pradhan, Á. Linares-Solano, D. Cazorla-Amorós, Semihydrogenation of phenylacetylene catalyzed by palladium nanoparticles supported on carbon materials, J. Phys. Chem. C 112 (2008) 3827–3834, https://doi.org/10.1021/jp710693u.
[68] A.V. Astakhov, O.V. Khazipov, A.Y. Chernenko, D.V. Pasyukov, A.S. Kashin, E. G. Gordeev, V.N. Khrustalev, V.M. Chernyshev, V.P. Ananikov, A new mode of operation of Pd-NHC systems studied in a catalytic mizoroki–heck reaction, Organometallics 36 (2017) 1981, https://doi.org/10.1021/acs.organomet.7b00184. –1992.
[69] D.B. Eremin, V.P. Ananikov, Understanding active species in catalytic transformations: from molecular catalysis to nanoparticles, leaching, "Cocktails" of catalysts and dynamic systems, Coord. Chem. Rev. 346 (2017) 2–19, https://doi.org/10.1016/j.ccr.2016.12.021.
[70] S.A. Yakukhnov, E.O. Pentsak, K.I. Galkin, R.M. Mironenko, V.A. Drozdov, V. A. Likholobov, V.P. Ananikov, Rapid "mix-and-stir" preparation of well-defined palladium on carbon catalysts for efficient practical use, ChemCatChem 10 (2018) 1869–1873, https://doi.org/10.1002/cctc.201700738.